Chemical Science

ROYAL SOCIETY OF CHEMISTRY

EDGE ARTICLE

View Article Online
View Journal | View Issue

Cite this: *Chem. Sci.*, 2025, **16**, 15086

All publication charges for this article have been paid for by the Royal Society of Chemistry

Tuning the emission properties of luminescent 1,2,3-diazaborinates†

Leonie Wüst,‡[ab] Johannes Chorbacher,‡[ab] Timo Keim,[ab] Tim Wellnitz,[ab] Julian Spieß,[ab] Nele Wieprecht,[ab] Maximilian Michel,[ab] Holger Helten *[ab] and Holger Braunschweig *[ab]

Received 26th May 2025
Accepted 28th June 2025

DOI: 10.1039/d5sc03814f

rsc.li/chemical-science

B-Aryl-based 1,2,3-diazaborinates (DABates), derived from neutral 1,2,3-diazaborines (DABs), are a promising class of unexplored fluorophores which show an intriguing high optical performance. This work systematically investigates previously unexplored factors that govern their photoluminescence. We strategically designed and synthesized a diverse library of DABate derivatives, modifying the exocyclic boron and N_α-substituents, the N_β-lone pair, and the fused π system. All compounds were fully characterized by conventional NMR, HRMS and XRD techniques, as well as UV-vis and fluorescence spectroscopy. Our results allow the identification of key molecular attributes which enhance or quench the fluorescence. Complementary supporting time-dependent DFT calculations provide further insights into the excitation process. In addition, we also performed modifications to render the DABates air- and moisture-stable, expanding potential future applications of this novel class of potent fluorophores beyond inert conditions.

Introduction

Fluorescence-based techniques, such as fluorescence spectroscopy,[1–3] cell labelling,[4–6] dye-assisted lasers[7] and luminescence chemosensing,[8–11] are indispensable tools of modern technology and depend on effective fluorophores. Although novel fluorophores often originate from a serendipitous discovery, subsequent modification and optimization of optical performance predominantly rely on the rational manipulation of key molecular attributes that promote fluorescence: as the fluorescence process is normally preceded by an excitation within the lower energetical region of UV or visible light, this criterion is met by the absorption region of larger aromatic π systems or non-bonding molecular orbitals.[12] In this context, n → π* transitions usually have a small transition probability due to insufficient n/π* orbital overlap and can additionally result in increased spin–orbit coupling, which promotes intersystem crossing and thus non-radiative decay.[13–15] In contrast, π → π* transitions usually feature considerably higher molar absorptivity due to conjugative effects along the main molecular axis. This can be further enhanced by extending the π system or combining electron-donating (D) and -accepting (A) substituents, where the latter supports the redistribution of electrons during the excitation in form of an intramolecular charge transfer (CT).[12]

Rigid molecular geometries are advantageous for this process and can be achieved by incorporating a chelated sp^3-hybridized boron atom, which effectively locks the configuration of the organic framework.[16–18] Prominent examples for boron-containing fluorophores that utilize this effect are the well-established boron dipyrromethene (BODIPY) derivatives, dating back to early works of Treibs and Kreuzer.[19] More recently, boron difluoride hydrazones (BODIHY), first synthesized by the group of Aprahamian,[20] and boron difluoride formazanate dyes (BF_2Fz) have emerged as other classes of fluorescent boron compounds, both of which are currently mainly advanced by Gilroy and coworkers (Fig. 1).[21–28] While common BODIPY dyes also feature a BF_2-group (R = F, F-BODIPY), other boron substituents such as carbocycles (R = Ar, C-BODIPY) or oxygen (R = OR, O-BODIPY) and backbone modifications are also reported and result in different optical properties.[29,30]

The incorporation of heavy atoms (S, Se, Te) in BODIPYs favors intersystem crossing (ISC) and a decreasing fluorescence quantum yield in accordance with heavy atom effects.[31] Likewise, by structurally modifying the organic periphery of the BODIHY or BF_2Fz dyes, their photoluminescence and redox

[a]*Julius-Maximilians-Universität Würzburg, Institute of Inorganic Chemistry, Am Hubland, 97074 Würzburg, Germany. E-mail: holger.helten@uni-wuerzburg.de; h.braunschweig@uni-wuerzburg.de*

[b]*Institute for Sustainable Chemistry & Catalysis with Boron, Am Hubland, 97074 Würzburg, Germany*

† Electronic supplementary information (ESI) available: General methods and materials, experimental procedures and characterization data, photophysical data, X-ray crystal structure determination and computational section. CCDC 2453528–2453546, 2453634 and 2453635. For ESI and crystallographic data in CIF or other electronic format see DOI: https://doi.org/10.1039/d5sc03814f

‡ These authors contributed equally to this work.

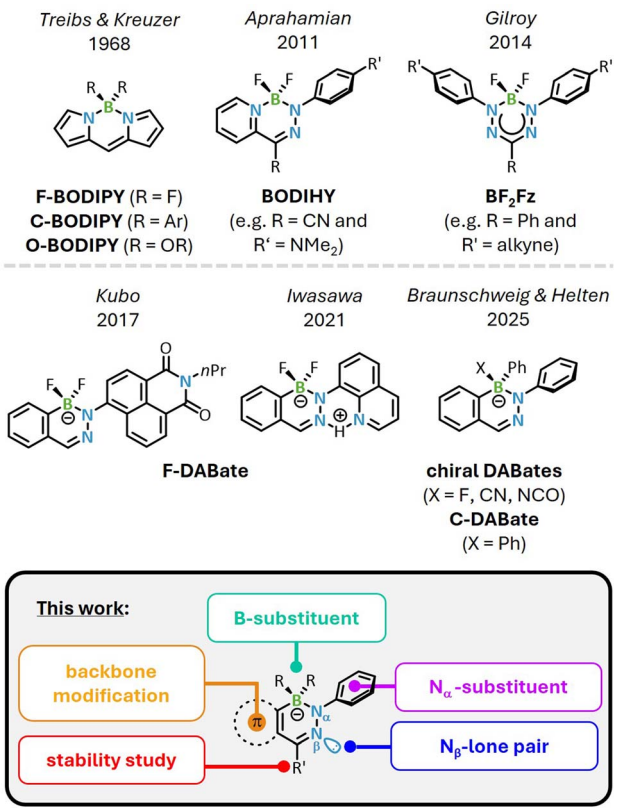

Fig. 1 Basic scaffolds of established BODIPY, BODIHY and BF_2Fz dyes (top), diazaborinates (DABates, middle) and investigated structure–properties relationships in this work (bottom).

properties can be tuned to enhance CT characteristics or show dual or aggregation-induced emission (AIE) behavior.[21–24]

Contrasting BODIHYs and BF_2Fzs, the field of structurally related, luminescent 1,2,3-diazaborinates (DABates) is still in its infancy and limited to very few reported examples. While a comparatively larger number of O-DABates, mostly featuring $B(OH)_2$-borates, is reported, they appear to be mostly non-emissive species.[32–35] In 2017, Kubo and coworkers synthesized the naphthalimide-appended F-DABate with BF_2-moiety as part of a fluoride (F^-) anion sensing study, though the group only focused on changes in the absorption spectra upon anion addition as well as the luminescence of the neutral precursor (Fig. 1, middle).[36] A few years later, the group of Iwasawa reported an F-DABate with a quinoline substituent, which was characterized as very weakly fluorescent in solution but showed an enhanced emission with AIE character in the crystalline solid state.[37]

Recently, our groups reported a synthetic access to B-aryl-substituted, neutral 1,2,3-diazaborines (DABs),[38,39] which are isoelectronic BN-congeners of isoquinolines and can act as highly sensitive fluorescence "turn-on" chemosensors. The sensing process is based on the formation of chiral, emissive DABates upon nucleophilic attack of the respective anion (F^-, CN^-) at the boron center, with quantum yields reaching up to $\Phi_{fl} = 80\%$ in a rigid environment. During our synthetic work on these neutral DABs, we also isolated an achiral, luminescent C-DABate, featuring a BPh_2-unit.[38] Intrigued by the optical performance of the borates formed, this work is aiming at systematically studying previously unexplored factors, which govern the photoluminescence of these DABates. For this purpose, we devised a strategic variety of system alterations on different positions of the DABate core, covering the exocyclic boron and N_α-substituents, the N_β-lone pair as well as the fused π system (Fig. 1, bottom). In addition, we performed modifications to also render the DABates air- and moisture-stable to pave the way for potential applications beyond Schlenk conditions. Our photochemical and stability studies are rationalized and supported by XRD studies as well as TD-DFT calculations.

Results and discussion

Syntheses of DABate derivatives

In analogy to the previously reported preparation of the parent C-DABate **5Ph[Li]** (parent compound in Scheme 1a, black),[38] we developed a general synthetic procedure for achiral C-DABates. To install different exocyclic boron substituents, we reacted **1OTMS** with a variety of organolithium reagents to obtain the C-DABates **5R[Li]** (Scheme 1a, right-hand side, green). The lithium organyls were either used in solid, solvent-free form (R = Me, Thio) or generated *in situ via* prior transmetalation of a bromo precursor with *n*-butyllithium in a one-pot synthesis (R = Ph, Biph, Cbz, OMe, CF_3). To prevent the formation of *n*-butylated side products (*e.g.* **5*n*Bu[Li]**) with similar solubility as the products **5R[Li]** due to a nucleophilic attack of excess transmetalation agent on **1OTMS**, we used slightly sub-stoichiometric amounts of *n*-BuLi in some cases. This results in lower yields of **5R[Li]** but has proven to be the best method for synthesizing the C-DABates, since potential side products such as the monosubstituted, neutral DAB species **1R** or remaining **1OTMS** are usually easily removed by washing with *n*-pentane.[38] We also found that the order of addition is crucial for the successful synthesis of **5R[Li]**. The addition of **1OTMS** to a solution of the respective lithium organyl leads to unselective reactions, presumably due to an additional attack of RLi on the electrophilic aldimine position of the DABate, as this order of addition generates an initial surplus of RLi during the addition of **1OTMS**. Consequently, such side reactions can be prevented by slow addition of RLi to a solution of **1OTMS**. While the reaction times and temperatures were varied slightly depending on the reactivity of the respective lithium organyl, the use of diethyl ether was essential in all cases. The diethyl ether-complexed DABates precipitate and can be isolated in high purity by filtration and washing. In contrast, the THF complexes of **5R[Li]** show increased solubility even in non-polar solvents such as benzene, which prevents purification by washing.

Taking these points into account, it was possible to prepare a wide range of different boron-substituted C-DABates **5R[Li]** in yields of 37–77%, with yield discrepancies mostly resulting from differences in solubility behavior, rather than unselective reactions. The substituents R^3 include alkyl or aryl groups (R = Me, Ph), electron-donating or -accepting groups (R = *p*-C_6H_4-OMe, *p*-C_6H_4-CF_3), the incorporation of a heavy atom (R = 2-thienyl) or additional fluorophores (R = 2,2′-biphenyl, *p*-C_6H_4-Cbz). Like the

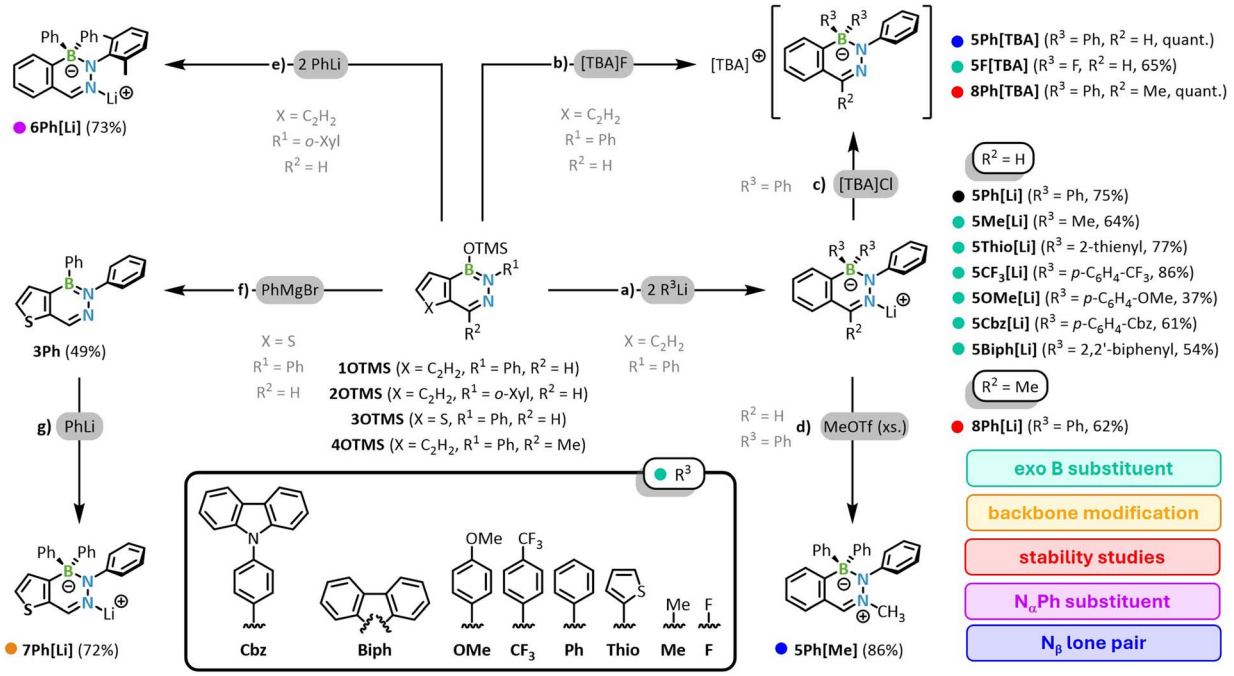

Scheme 1 Rational synthetic manipulation of key attributes, based on the parent compounds **5Ph[Li]** and **5Ph[TBA]**. (a) Installing carbon-based, exocyclic boron substituents (R^3) of varying electronic properties using different lithium organyls and a ketimine instead of an aldimine derivative for stability studies (Et_2O, −78 °C → rt or rt, 16 h or 32 h); (b) installing fluoride-based, exocyclic boron substituents using [TBA]F (THF, 80 °C, 4 d); (c) salt metathesis to separate ion pairs (THF, sonification, rt, 1 h); (d) methylation of the N_β-position with an excess of methyl triflate to a zwitterionic salt (MeCN, rt, 16 h); (e) synthesis of a derivative with a sterically demanding N_α-substituent (Et_2O, rt, 16 h); (f) (CH_2Cl_2, rt, 16 h) and (g) (Et_2O, rt, 16 h) synthesis of a derivative with a different backbone π system *via* its neutral phenyl-DAB (Ph = phenyl; *o*-Xyl = *ortho*-2,6-dimethylphenyl; Cbz = 9*H*-carbazole; OTf^- = triflate; TBA = tetra-*n*-butylammonium). Respective changes on the parent compound **5Ph[Li]** (black) are color coded.

parent compound **5Ph[Li]** and the anion sensing compounds from our previous work (*cf.* Fig. 1),[38] all DABates show the expected high-field shift of the sp^3-boron in the ^{11}B NMR spectra compared to the precursor **1OTMS** ($\delta(^{11}B) = 27$ ppm). In contrast to the sensing DABates, the individual diazaborinates **5R[Li]** hardly differ in their ^{11}B NMR resonances and are detected in the range from −3.1 to −7.1 ppm. For compounds **5Me[Li]** and **5Thio[Li]**, with substituents that can be classified as comparatively electron-rich, a slightly more pronounced high-field shift is observed compared to the phenyl-substituted DABates. Similarly, the strongest high-field shift for the characteristic DABate aldimine proton (*H*-1) is also detected for **5Me[Li]** ($\delta(H\text{-}1) = 6.92$ ppm). Overall, however, no clear NMR spectroscopic trends can be determined for the different B-substitution patterns.

Inspired by the F-BODIPY family, as well as the F-DABates by Kubo and Iwasawa,[36,37] we also synthesized the fluoro-substituted F-DABate **5F[TBA]** from the reaction of **1OTMS** with [TBA]F in good yields of 65% after reflux in THF for four days (Scheme 1b, upper right corner, green). Due to the strong electron-withdrawing effect of the fluoro substituents, compound **5F[TBA]** exhibits a significantly low-field shifted ^{11}B NMR resonance compared to the other DABates at +3.4 ppm.

As the lithium DABates feature a complexation of the Li^+ cation by the N_β-atom of the DABate (*vide infra*), we were also interested in an in-depth study of the influence of the electronic situation at N_β on the photophysical properties. Our previous work demonstrated that the cation exchange TBA salt **5Ph[TBA]** (Scheme 1c, upper right corner, blue) of the parent DABate **5Ph[Li]** shows significantly different photophysical properties (*vide infra*).[38] To further investigate the influence of the N_β-lone-pair availability, we methylated the N_β-position in a metathesis reaction of **5Ph[Li]** with methyl triflate to the zwitterionic compound **5Ph[Me]** (Scheme 1d, lower right corner, blue). ^1H NMR spectroscopy reveals a strong electronic impact of the introduction of the positive charge on the BN_2C_3-ring, as the aldimine (*H*-1) resonance is experiencing a low field shift of *ca.* 1 ppm upon methylation ($\delta(H\text{-}1,$ **5Ph[Li]**$) = 7.11$ ppm).

As the structural conformation of a fluorophores' adjacent aromatic group such as the DABates N_α-Ph substituent often strongly impacts the photoluminescence,[40,41] we also synthesized compound **6Ph[Li]** with an N_α-*o*-xylyl (2,6-dimethylphenyl) instead of the N_α-Ph substituent (Scheme 1e, upper left corner, purple). In **6Ph[Li]**, the free rotation of the N_α-aryl is effectively blocked by the *ortho*-methyl groups (*cf.* calculated rotational barrier of *ca.* 26 kcal mol^{-1} for N_α-xylyl *vs. ca.* 7 kcal mol^{-1} for N_α-phenyl, ESI Fig. S114 and S115†), leading to an almost perpendicular arrangement to the central DABate core (*vide infra*).

Lastly, direct alterations of a fluorophores' π system, *e.g.* by replacing a carboaromatic group with a thiophene-fused counterpart, often induces significant changes in the photophysical properties.[42–45] While benzannulated DABs represent the

currently predominant DAB derivatives, early reports by Gronowitz and Bugge inspired us to synthesize the thiophene-fused DABate **7Ph[Li]** (Scheme 1g, lower left corner, yellow).[46] Since direct borate formation from **3OTMS** was not successful, we adapted our previously established procedure for the synthesis of neutral, aryl-substituted DABs to the thiophene-fused derivative. Thereby, we managed to isolate the intermediate product **3Ph** and subsequently converted **3Ph** to the corresponding DABate by treatment with PhLi, which allowed isolation of analytically pure **7Ph[Li]** in good yield of 72%.

Solid-state structures

Single-crystal X-ray diffraction (XRD) experiments were performed on all DABates shown in Scheme 1. Most of the derivatives exhibit distinctive 2- or 3-fold whole-molecule disorders in the solid-state, which are likely a result of molecular horizontal mirror planes and limit a detailed bond parameter discussion to approximated values for the most relevant derivatives (Table 1). Visualized examples of these disorders can be found in the ESI appendix (Fig. S113†) to explain the restrictions on a detailed bond discussion. Fig. 2 depicts the solid-state molecular structures of **5Ph[TBA]** (no N_β → cation complexation), **5Ph[Li]** (intact N_β → Li^+ coordination), **5Ph[Me]** (methylated N_β), and **6Ph[Li]** (*o*-xylyl substituent at N_α).

In comparison to the other three derivatives, the TBA salt of **5Ph** (Fig. 2a) with a free lone pair at the N_β shows a significantly more planarized BN_2C_3 core as well as a nearly co-planarized N_α-phenyl substituent. In contrast, all DABates with a blocked lone pair, either by Li^+ complexation or methylation, feature a strongly distorted BN_2C_3 half-chair core with the BR_2 unit bending out of the remaining DABate plane. To quantify this distortion, we defined the angle φ (Table 1, inset) which reflects this twisted nature by high values of 25–44° for the parent compound **5Ph[Li]**, the N_β-methylated **5Ph[Me]**, and N_α-*o*-xylyl derivative **6Ph[Li]** (*cf.* TBA salt of the parent DAB with free N_β φ(**5Ph[TBA]**) = 10°). The N_β–N_α–C1–C2 torsion angle serves as an additional indicator for the co-planarization of the respective N_α substituent. Comparison of this angle for all DABates gives the same trend as the bent angle φ: the derivatives **5Ph[Li]** (parent DABate), **5Ph[Me]** (N_β methylated), and **6Ph[Li]** (*o*-xylyl-N_β) also exhibit the most twisted N_α substituents to accommodate the spatial requirements of the Li^+ cation.

Here, the *o*-xylyl derivative **6Ph[Li]** shows the highest angle of 61° and an elongated N_β → Li bond due to the additional steric effects of the *ortho*-methyl groups. Interestingly, in direct comparison to the other Li^+ coordinating DABates, the thiophene-fused compound **7Ph[Li]** shows a relatively planarized geometry with bond parameters in a similar range as the TBA salt of the parent DAB **5Ph[TBA]**, despite the intact N_β → Li coordination. F-DABate **5F[TBA]** features the most planarized geometry of all DABates in this study, since the small F substituents in combination with the TBA counter cation minimize the steric constraints on the system. The B–N_α bond in **5F[TBA]** of *ca.* 1.52 Å is also significantly contracted in comparison to the C-DABates, as the electron-withdrawing F-substituents retain a more Lewis-acidic boron center, which is compensated for by the non-bonding lone-pair of the adjacent N_α atom. In contrast, all C-DABates feature strikingly long B–N_α bonds of *ca.* 1.59–1.62 Å, despite their incorporation in a cyclic system (*cf.* 1.4210(19) Å for the neutral phenyl DAB **1Ph**). While elongated B–N_α bonds in the B(sp^3)-hybridized DABates

Table 1 Selected bond lengths, and angles of selected DABates, with the B out-of-plane distortion angle φ as a measure of DABate ring distortion and the N_β–N_α–C1–C2 torsion angle as an indicator of N_β-substituent coplanarity

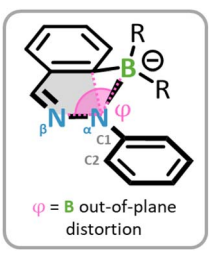

No.	Modification	N_β → Li^a [Å]	B–$N_\alpha{}^a$ [Å]	φ [°]	N_β–N_α–C1–C2^a [°]
● **5Ph[Li]**	—	2.02	1.58	33	36
● **5Ph[TBA]**	Cleaved N_β-cation interaction	—	1.59	10	16
● **5Ph[Me]**	N_β methylation	—	1.60	40	38
● **6Ph[Li]**	N_α xylyl substituent	2.18	1.60	25	61
● **7Ph[Li]**	Thiophene-fused backbone	2.04	1.62	10	28
● **8Ph[Li]**	Ketimine	2.06	1.58	29	29
● **8Ph[TBA]**	Ketimine	—	1.59	21	11
● **5F[TBA]**	Fluoro substituents at boron	—	1.52	4	4

[a] Due to the presence of major whole molecule disorders for most of the derivatives, only rounded values are discussed. For exact bond data on non-disordered derivatives see ESI.

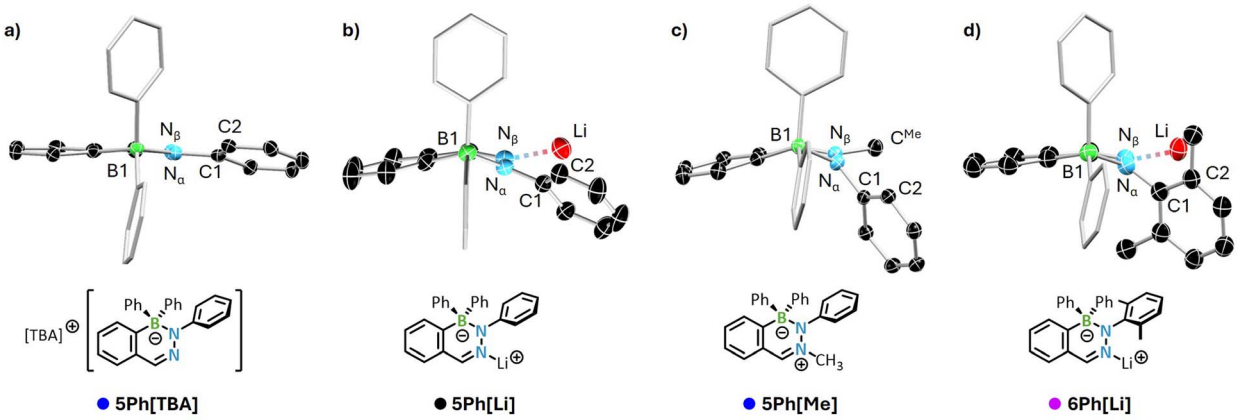

Fig. 2 Molecular structures of selected DABates (a) **5Ph[TBA]**, (b) **5Ph[Li]**, (c) **5Ph[Me]**, and (d) **6Ph[Li]** in top view. Ellipsoids drawn at 50% probability (100 K). Complexing ether or tetrahydrofuran molecules and hydrogen atoms omitted for clarity. Phenyl substituents at the boron atoms rendered as wireframe. TBA counter ion omitted for **5Ph[TBA]**. For selected bond parameters see Table 1. For the solid-state structures in side view of these compounds and the other DABates derivatives structures in side view of these compounds and the other DABates derivatives see the ESI.†

compared to the neutral B(sp^2)-DABs are generally to be expected due to the loss of π character, such drastic differences raise doubts as to whether the B–N_α bond can still be described as a single bond without dative participations. However, calculated NBO and Mulliken charges give unambiguous information that contradicts such a description (ESI, Table S4†). No additional information or trends can be extracted from the comparison of the other B-substituted derivatives **5R[Li]**. All solid-state structures and bond parameters, if permitted by the absence of disorders, are provided in the ESI.†

Photophysical properties

We investigated the photophysical properties of all compounds by UV-vis absorption and fluorescence emission spectroscopy in solution and as PMMA films. For a more comprehensive comparison, we also include data for the parent compound **5Ph[Li]** and its TBA congener **5Ph[TBA]** in our discussion, which we have recently reported.[38] The UV-vis spectra of the very low or non-emitting neutral DABs **1R–4R** all show a maximum of the lowest-energy absorption band between 300–307 nm in THF, which demonstrates that the modification of the precursor has no major influence on the absorption properties (ESI, Table S3†). Compared to the neutral DABs, the DABates show a clear bathochromic shift of up to 111 nm. Depending on the respective variation of the parent structure, compounds **5R–8R** (except from F-DABate **5F[TBA]**) show a slight wavelength shift of the lowest-energy absorption bands from 390–415 nm (ESI, Table S4†). Particularly striking here is the hypsochromic shift of the F-DABate **5F[TBA]**, which shows a maximum at 355 nm, thus following the trend of the recently reported chiral DABate (Fig. 1, X = F) (369 nm) and **5Ph[TBA]** (398 nm).[38] Based on TD-DFT calculations of the vertical singlet excitations of the DABate compounds, we assign the lowest-energy absorptions to a π–π* process, which, except for **5Cbz** with carbazole substituents, corresponds to a HOMO → LUMO excitation (*vide infra*).

The unexpectedly pronounced fluorescence of the parent DABate **5Ph** and the resulting sensor application of the precursor **1Ph** has already been characterized in our recent work.[38] This follow-up study aims to investigate the mechanism of the fluorescence and the influence of molecular modifications to **5Ph** on the emission properties of this novel class of substances (*vide supra*). We began our investigations by varying the boron substituents. For this purpose, we attached substituents with electron-donating (**5OMe[Li]**) or -withdrawing (**5CF_3[Li]**) properties, an extended π system (**5Cbz[Li]**), a rigid geometry (**5Biph[Li]**), a heteroaromatic ring (**5Thio[Li]**) or sterically varying (**5F[TBA]**, **5Me[Li]**) substituents to the boron atom. Except for **5F[TBA]** and **5Me[Li]**, all differently substituted C-DABates show similar properties in solution and in the PMMA film (see ESI, Table S4 and Fig. S140†). They display a narrow emission curve in THF and the PMMA film, which is mirror-inverted to their lowest-energy absorption bands, with quantum yields of Φ_{fl} = 12–19% in THF and Φ_{fl} = 25–42% in the film (Fig. 3 and Table 2; for all data, see Table S4 in the ESI†).

In toluene, however, only a quenched, bathochromically shifted and weak emission is present for all lithium DABates. As we have already shown, the counterion has a major impact on the properties in solution (see **5Ph[Li]** and **5Ph[TBA]**).[38] We reasoned that the cleavage of the N_β → Li coordination by formation of solvent-separated ion pairs [DABate][Li(thf)$_n$] in THF is responsible for the emission in THF, whereas the N_β → Li coordination should remain intact in toluene due to the absence of additional donor molecules. These observations suggest that the N_β lone pair has an important influence on the emission behavior of the compounds. To verify this, we substituted the N_β of **5Ph[Li]** with a methyl group to form **5Ph[Me]**, which completely quenched the emission. This behavior of the DABates is therefore contrary to that of the related, parent CC-compound isoquinoline, which shows a clear increase in fluorescence when protonated at nitrogen.[13]

When comparing the compounds **5R** (excluding the non-emissive compound **5Ph[Me]**), it is striking that the DABates with small fluoro or methyl substituents at the boron **5F[TBA]** and **5Me[Li]** exhibit very low fluorescence in solution but with

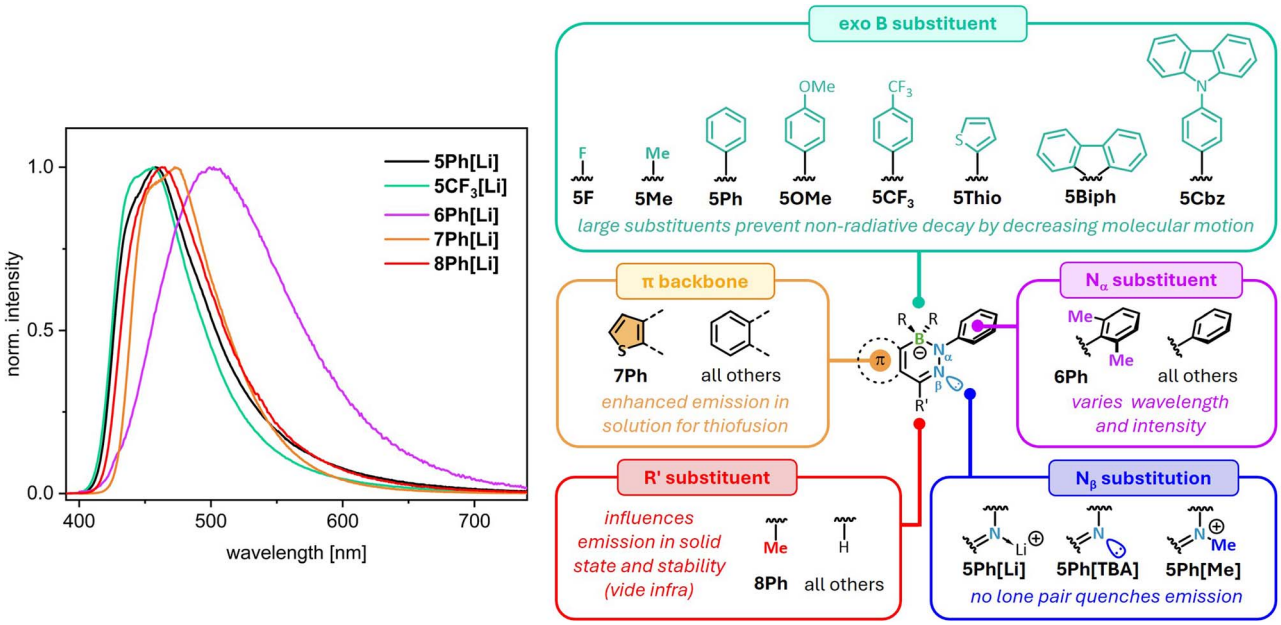

Fig. 3 Normalized emission spectra of **5Ph[Li]**, **5CF3[Li]**, **6Ph[Li]**, **7Ph[Li]**, and **8Ph[Li]** in THF. Inset: overview of structural factors influencing emission.

Table 2 Photophysical data of selected compounds **5Ph[Li]**–**8Ph[Li]** in THF, toluene and as PMMA film

No.	$\lambda_{abs,max}$ [a] [nm]	$\lambda_{abs,max}$ [b] [nm]	$\lambda_{abs,max}$ [c] [nm]	$\lambda_{em,max}$ [a] [nm]	$\lambda_{em,max}$ [b] [nm]	$\lambda_{em,max}$ [c] [nm]	Φ_{fl} [a,d] [%]	Φ_{fl} [b,d] [%]	Φ_{fl} [c,d] [%]	τ_{fl} [a] [ns]
5Ph[Li]	398	396	391	460	455	510	18	30	—	1.70; 2.57
5Ph[TBA]	398	399	404	459	463	479	19	27	8	1.63; 2.57
5Ph[Me]	415	—	421	—	—	—	—	—	—	—
5CF$_3$[Li]	395	391	388	453	445	529	19	42	—	—
5Cbz[Li]	397	395	390	456	451	510	12	34	—	1.65; 2.34
5F[TBA]	355	354	354	428	427	—	—	37	—	—
6Ph[Li]	390	387	393	501	483	504	7	3	—	2.16; 3.61
7Ph[Li]	410	410	411	465	477	490	63	28	—	5.63
8Ph[Li]	403	402	410	463	463	489	26	5	—	2.96

[a] THF. [b] PMMA film. [c] Toluene. [d] Fluorescence quantum yields, determined using an integration sphere.

simultaneously intensified fluorescence compared to the other derivatives in this series in rigid PMMA film. This behavior indicates an aggregation-induced emission effect similar to the BODIHY or BF_2Fz dyes.[23–25] Thus, the lower steric demand of the boron substituents could enhance molecular motions, especially for the Ph group attached at the N_α position, which results in more efficient non-radiative relaxation processes. To prove this experimentally, we investigated the behavior of fluoro compound **5F[TBA]** in DMSO, which led to an intensification of the emission and a decrease in intensity of the broad bathochromically shifted band of the dual emission (Fig. 4). However, since the compound is sensitive to hydrolysis, conventional AIE experiments, in which aggregation and thus hindered molecular motion through the hydrophobic character of the compound is forced by increasing the water content of a dissolved sample, cannot be performed. As **5F[TBA]** does not dissolve in *n*-pentane, we tested samples with different THF/*n*-pentane ratios to investigate this effect. When *n*-pentane (up to 90%) was added to a THF solution of the F-DABatee, a clouding of the sample was observed and the fluorescence intensity increased *ca.* 94-fold relative to the pure THF solution (Fig. 4). Since molecular movements can also be restricted by cooling, which increases the viscosity, we monitored the emission intensity as a function of temperature in the range from 303 to 103 K in 2-MeTHF. By cooling to 103 K, an increase in intensity by a factor of 80 was observed (Fig. 4). Similar to the observations for the measurements in THF and DMSO, the intensity of the bathochromic band decreases with decreasing temperature until it is no longer visible beyond the glass transition temperature of 2-MeTHF (137 K) at 133 K (Fig. S129 in the

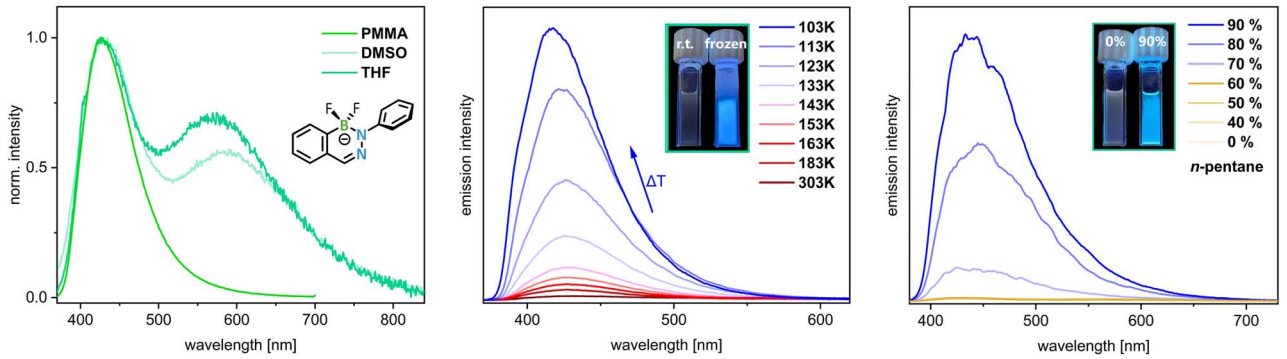

Fig. 4 Emission spectra of **5F[TBA]** in different solvents (left), variable-temperature emission spectra of **5F[TBA]** in 2-MeTHF from 303 to 103 K (middle), and emission spectra of **5F[TBA]** in THF/*n*-pentane mixtures (conc. 5×10^{-5} M). Inset: structure of the compound and corresponding samples under UV light.

ESI†). These observations suggest that a bulky residue on boron is favorable for efficient emission in solution but is not necessary in a rigid environment or in the solid state. To further explore the aggregation behavior of **5F[TBA]**, we prepared various PMMA films with different DABate contents (0.025–2.5 mg). With increasing contents of the PMMA matrices, a bathochromic shift of the bands from $\lambda_{em,max} = 418$ nm to 432 nm was observed (ESI, Fig. S132†). In solution, an increase in concentration led to quenching of the fluorescence. From these results it could be concluded that an aggregation effect such as π–π stacking may be present in the rigid films.

The comparison of the XRD structures with the photophysical data suggests that the planarity of the backbone and the position of the freely rotatable N_α-Ph group plays a decisive role for the fluorescence behavior. For example, in the solid-state structure of the non-emissive, N_β methylated DABate **5Ph[Me]**, a strong twisting of the backbone and the N_α-Ph group is observed. In contrast, the F-DABate **5F[TBA]** is approximately planar in the solid state. This planar conformation is enforced by increasing the viscosity or in the rigid environment of the PMMA film, leading to a significant intensification of the emission (Fig. 4). To restrict rotation, we have installed the bulkier *o*-xylyl group at the N_α-position (**6Ph[Li]**). The result of this modification was a significantly lower emission intensity both in solution ($\Phi_{fl} = 7\%$) and in the PMMA film ($\Phi_{fl} = 3\%$) and a broadening and bathochromic shift of the fluorescence band (Fig. 3 and Table 2). This can be attributed to the almost perpendicular arrangement of the *o*-xylyl group to the DABate core and the associated low involvement in the emission process (*vide infra*).

In addition, we tested the modification of the π backbone by exchanging the benzannulated system with a fused thiophene system, resulting in **7Ph[Li]** (Scheme 1). While similar fluorescence behavior of **7Ph[Li]** is observed in the PMMA film in comparison to the benzannulated **5R[Li]** compounds, a significantly increased quantum yield of up to 63% is found in solution (Table 2). This shows that the π backbone also has a significant influence on the emission behavior and thus provides a useful strategy for future, fluorescence enhancing modifications.

As a final modification, we prepared a DABate with a methyl group at the imine position (*i.e.* **8Ph[Li]** and **8Ph[TBA]**) to achieve higher stability (*vide infra*). Here, both compounds show an increased quantum yield of $\Phi_{fl} = 26\%$ in solution (compared to $\Phi_{fl} = 18\%$ for the parent compound **5Ph[Li]**), but a lower quantum yield in the PMMA film.

Computational studies

Density functional theory (DFT) calculations were performed on all DABates using the Gaussian 16 program (see ESI† for computational studies of all compounds).[47] All calculations were carried out on the free DABates without inclusion of the corresponding countercations (ωB97X-D[48]/def2-SVP,[49] see ESI†). In general, the calculated geometries exhibit less twisting and deplanarization compared to the solid-state structures (*vide supra*). This discrepancy is likely due to the absence of the Li^+ coordination, which mimics the photoemissive situation upon THF solvation. Similar to the parent compound **5Ph**$^-$, the highest occupied molecular orbital (HOMO) of all DABate derivatives features a nodal plane between the N_α and the boron atom, with the orbital coefficient at the N_α resembling p_z character (Fig. 5). Both the HOMO and the lowest unoccupied molecular orbital (LUMO) display π symmetry. The HOMO–LUMO energy gaps of all DABates (except **5Cbz**$^-$, *vide infra*) fall within the range of 7.2–7.5 eV.

The photoabsorption properties of all derivatives were also investigated using time-dependent (TD-DFT) methods

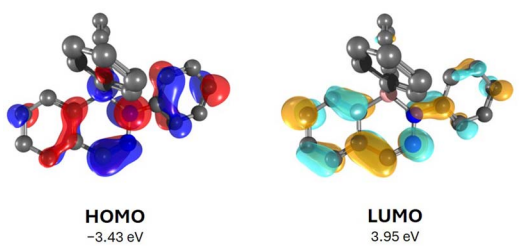

Fig. 5 Exemplary frontier molecular orbitals (FMOs) of the parent compound **5Ph**$^-$ (ωB97X-D/def2-SVP/isovalue 0.06 eÅ^{-3}).

Table 3 Calculated electronic excitations with the largest oscillator strength and experimental absorption maxima of all DABates (tHCTHhyb/def2-TZVPP/solvent = tetrahydrofuran/td(nstates = 10))

No.	Transition	λ_{exp} [nm]	λ_{calc} [nm]	Main excitation
● **5Ph**$^-$	$S_0 \rightarrow S_1$	398	401	HOMO → LUMO
● **5F**$^-$	$S_0 \rightarrow S_1$	355	364	HOMO → LUMO
● **5Me**$^-$	$S_0 \rightarrow S_1$	404	415	HOMO → LUMO
● **5Thio**$^-$	$S_0 \rightarrow S_1$	388	392	HOMO → LUMO
● **5CF$_3$**$^-$	$S_0 \rightarrow S_1$	395	404	HOMO → LUMO
● **5OMe**$^-$	$S_0 \rightarrow S_1$	398	401	HOMO → LUMO
● **5Biph**$^-$	$S_0 \rightarrow S_2$	404	409	HOMO → LUMO
● **5Cbz**$^-$	$S_0 \rightarrow S_3$	397	402	HOMO → LUMO+2
● **6Ph**$^-$	$S_0 \rightarrow S_1$	390	399	HOMO → LUMO
● **7Ph**$^-$	$S_0 \rightarrow S_1$	410	421	HOMO → LUMO
● **8Ph**$^-$	$S_0 \rightarrow S_1$	403	406	HOMO → LUMO
● **5Ph[Me]**	$S_0 \rightarrow S_1$	415	443	HOMO → LUMO

(tHCTHhyb[50]/def2-TZVPP[49,51]) in a solvent model mimicking tetrahydrofuran solvation. All values are in good agreement with the experimental values (Table 3).

For all DABates, except for **5Cbz**$^-$ with additional carbazole substituents, the primary electronic transitions correspond to HOMO(π) → LUMO(π^*) excitations. In case of **5Cbz**$^-$, the presence of the incorporated carbazole units results in the LUMO and LUMO+1 being centered on the carbazole moiety. Consequently, the main electronic excitation is the HOMO(π) → LUMO+2(π^*) transition, with the LUMO+2 resembling the LUMO situation of the other DABates (ESI, Fig. S124†). Except for **5Cbz**$^-$ and **5Biph**$^-$, reminiscent of a borafluorene, all transitions correspond to $S_0 \rightarrow S_1$ excitations. Geometry optimization of the first excited S_1 state of the parent compound **5Ph**$^-$ revealed a minor geometric change upon electronic excitation (Fig. 6), reminiscent of the phenomenon of planarity-induced CT.[52] While the S_0 ground state exhibits a bent DABate BN_2C_3 core and a consequently slightly out-of-plane twisted N_α–Ph substituent, the DABate in the optimized S_1 geometry is fully planarized with a co-planar N_α–Ph substituent.

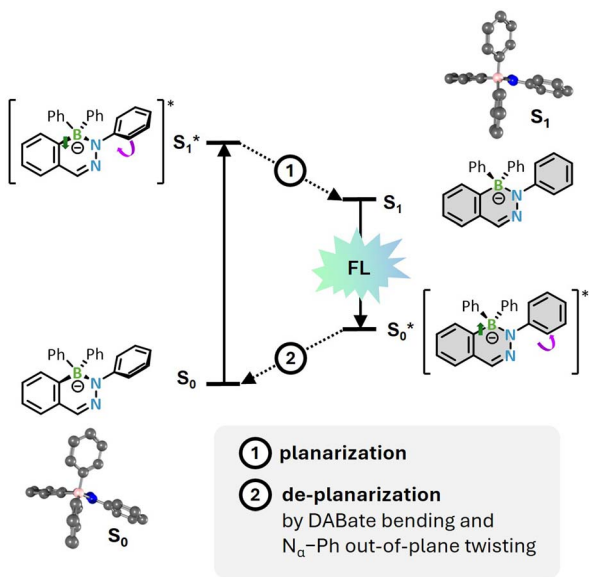

Fig. 6 Schematic depiction of the geometric changes during the excitation and relaxation of the model DABate **5Ph**$^-$ (grey = planarized).

To gain a deeper understanding of the photophysical differences observed for the key compounds **5Ph**$^-$ (parent C-DABate), **6Ph**$^-$ (N_α-*o*-xylyl), **7Ph**$^-$ (thiophene-fused) and **5Ph[Me]** (N_β methylated), we analyzed the transition character of the first singlet excited state (S_1), using the Multiwfn program (see ESI, section 4†).[53,54] The visualized electron–hole distributions of **5Ph**$^-$ and thiophene-fused **7Ph**$^-$ revealed an overall dominant intramolecular CT character of 70–73%, with the N_α-Ph substituent acting as an electron donor for the DABate acceptor unit (Fig. 7). For this transition, the central BN_2C_3 ring appears to serve as a bridging connection with both electron and hole contributions that correspond to a local excitation (LE) of 39–43%. Interestingly, the boron atom is completely excluded from the transition in both cases, explaining the minor influence of the C-DABates exocyclic boron substituents on the photophysical properties. In **6Ph**$^-$, the N_α-xylyl substituent adopts a perpendicular orientation to the DABate, which effectively excludes the N_α substituent from the transition. This reduces the CT character to 63% with simultaneously high LE character of 44% for the transition from the BN_2C_3 unit to the benzannulated system and is experimentally reflected in the comparatively lower quantum yield of **6Ph**$^-$ (*vide supra*). Similarly, in the N_β-methylated **5Ph[Me]**, the N_α-substituent is also noticeably twisted out of the DABate plane. However, unlike **6Ph**$^-$ with N_α-*o*-xylyl substituent, the hole remains located on the N_α-phenyl substituent, which likely contributes to the compounds non-emissive character. Unlike their distant CC-isoquinoline relatives,[13] no relevant n → π^* transitions involving the N_β-lone pair are found for the DABates (*vide supra*), despite its drastic influence on the photoluminescence. This prompted us to further analyze the interfragment CT in search of an alternative explanation for the quenching effect of the N_β-methylation or lithium coordination. Both modifications significantly lower the electron density in the central DABate unit, as evidenced by a substantially lower net amount of 0.18 e^- transferred from the BN_2C_3 ring to the benzannulated system for the N_β-methylated **5Ph[Me]** (*cf.* 0.25 e^- for parent compound **5Ph**$^-$, 0.27 e^- for thiophene-fused **7Ph**$^-$ and 0.30 e^- for N_α-*o*-xylyl **6Ph**$^-$). Hence, the quenching is likely a result of electron deprivation in combination with a sterically hindered in-plane rotation of the N_α-Ph substituent in **5Ph[Me]** and the DABate lithium complexes.

Stability studies

Given that the C-DABates of this work represent a potent class of novel fluorophores, the question of their air- and moisture-stability seems consequential for practical use. We additionally investigated the photostability of selected compounds (**5Ph[TBA]**, **5F[TBA]**, **7Ph[Li]** and **8Ph[TBA]**) by irradiation with an UV lamp at 254 and 365 nm. In THF solution, complete decomposition was observed after 90 min. In contrast, no noticeable

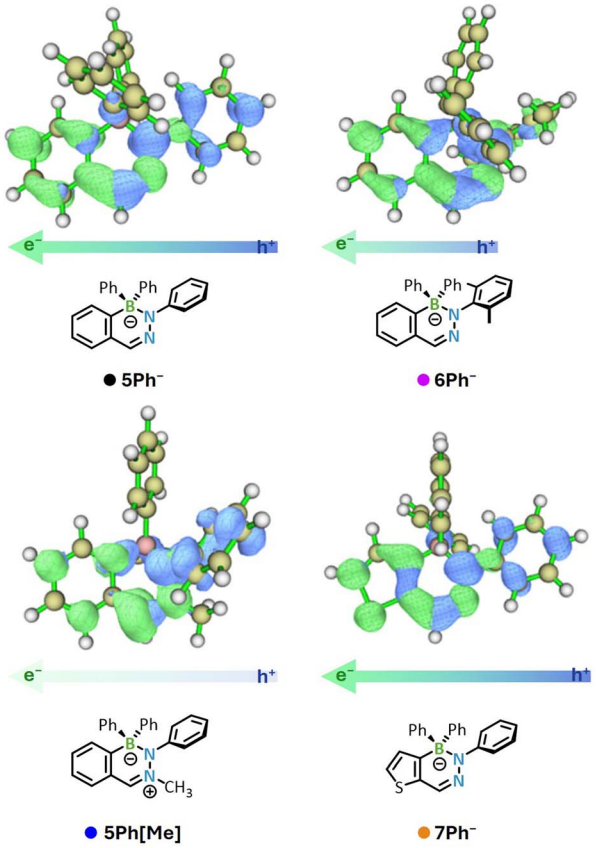

Fig. 7 Simultaneous isosurface of the electron (e^-, green) and hole (h^+, blue) distribution of **5Ph**$^-$, **6Ph**$^-$, **7Ph**$^-$ and **5Ph[Me]** for the $S_0 \rightarrow S_1$ transition density analysis (isovalue 0.02 a.u.).

change was detected when powders of the compounds were irradiated, rendering the DABates susceptible towards photolysis in solution but stable in the solid state. Following their synthesis under inert Ar atmosphere and Schlenk conditions, we noticed that solutions of all DABates their color from neon yellow to deep red within hours upon opening the reaction vessels to the atmosphere (Fig. 8a). This slow color change is accompanied by a rapid emission quenching as soon as the solutions are exposed to air. To understand the underlying degradation process, we separately reacted the isolated parent compound **5Ph[Li]** with dry O_2, as well as degassed H_2O. While the addition of H_2O resulted in a quenched emission, likely due to the formation of **5Ph[H]** and LiOH in analogy to the non-emissive methylated compound **5Ph[Me]** (*vide supra*), no color change to deep red was observed. In contrast, the reaction with dry O_2 gas resulted in a deep red-violet reaction mixture after a few hours. While monitoring the O_2 oxidation by ^{1}H and ^{11}B NMR spectroscopy revealed a highly unselective degradation reaction involving multiple species, one of which was confirmed as the neutral, monosubstituted DAB **1Ph**, we managed to identify compound **9** as one of the other oxidation products *via* XRD analysis (Fig. 8b and ESI, Fig. S107†).

The formation of **9** seems to be the result of an oxidative coupling of two DABates, which at some point of the reaction

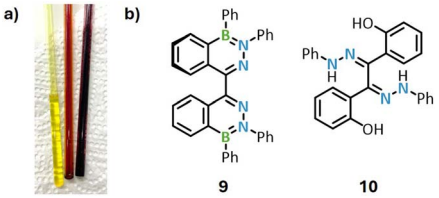

Fig. 8 (a) NMR samples of a DABate before (left, yellow solution) and after (middle and right, red solutions) atmosphere exposure. (b) Compounds **9** and **10** crystallized as part of the decomposition studies (for XRD structures see ESI, appendix Fig. S107 and S108†).

sequence rearomatized to the neutral DAB species by the loss of one of the exocyclic B–Ph substituents. A similar oxidative radical coupling is documented for structurally similar BODIHYs systems by Gilroy and coworkers.[24] While **9** would be interesting for potential follow-up studies as an atropisomeric ligand comparable to other binaphthyls (*e.g.* (*R*/*S*)-BINAP[55]), we were not able to fully characterize or selectively synthesize **9** despite extensive efforts (ESI, Table S2†). However, we also obtained single crystals of compound **10** from a combined study with H_2O and O_2, which appears to be a final oxidation and hydrolysis product of this degradation pathway (Fig. 8b and ESI, Fig. S108†). The formation of **10** is reminiscent of the archetypal reaction of neutral DABs with reactive oxygen species (ROS) such as H_2O_2 and might indicate the formation of ROS during the decomposition process.[56]

Considering these results, we conceived stability enhancing modifications of our DABate systems. The formation of quenched **5Ph[H]** as a result of hydrolysis seemed preventable by utilizing the TBA salts of our DABates. A hydrolysis study of **5Ph[TBA]** under Ar atmosphere confirms this consideration, as no decomposition was observed *via* ^{1}H NMR spectroscopy even after 15 d in a 1 : 1 D_2O/THF-d_8 mixture (ESI, Fig. S109 and S110†). We then proceeded to address the problem of the

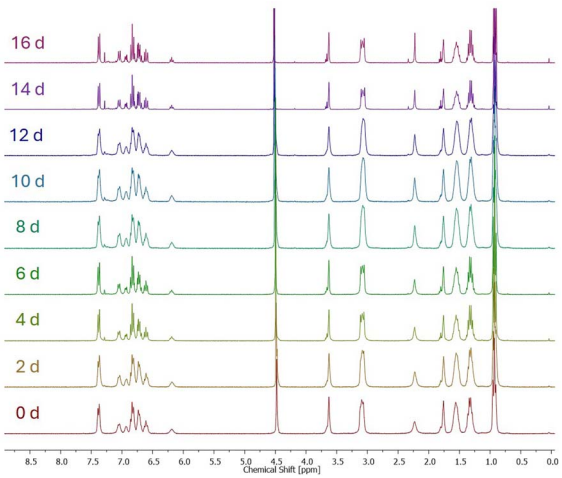

Fig. 9 Stacked ^{1}H NMR spectra of **8Ph[TBA]** in a 1 : 1 D_2O/THF-d_8 mixture under air over a period of 16 d, showing no significant decomposition.

observed oxidative coupling to species like **9** and **10** by synthesizing DABate **8Ph[TBA]**, featuring a ketimine ($N_\beta = C(CH_3)$) instead of an aldimine functionality ($N_\beta = C(H)$) at the central BN_2C_3 ring (Scheme 1, upper right corner). A ^{1}H NMR study of **8Ph[TBA]** in a 1 : 1H_2O/THF-d_8 mixture left open to the atmosphere showed no significant decomposition over the course of 15 d (Fig. 9 and ESI, Fig. S111 and S112†). This confirms the air- and moisture-stability of **8Ph[TBA]**, which is additionally demonstrated by growing the single crystals of **8Ph[TBA]** for XRD analysis from a THF/H_2O mixture under aerobic conditions (ESI Fig. S106†).

Conclusion

In this work we have carried out a comprehensive study on the structural, photophysical and electronic behavior of a series of unprecedented diazaborinates (DABates). For this purpose, we have synthesized a diverse library of DABate derivatives with specific modifications, including the exocyclic boron and Nα-substituents, the N_β-lone pair as well as the fused π system and the imine position. Our investigations showed that the lone pair at the N_β position plays an important role for the planarity of the compounds in the solid state. While DABates with a free lone pair adopt a nearly planar arrangement and co-planarized N_α-Ph group, lithium coordination or methylation leads to twisting of the entire molecular framework. Our photophysical investigations revealed that the N_β lone pair also has a major influence on the emission behavior. As shown by measurements in toluene, the fluorescence is quenched when the lithium is coordinated to the N_β of the DABates. However, it reveals emission again when the counterion is exchanged for TBA, resulting in the formation of separated ion pairs. By selectively substituting this site with a methyl group, the emission is extinguished in all media, which confirmed our assumption. Varying the exocyclic boron substituents had no significant effect on the fluorescence when measured in the rigid PMMA film. Meanwhile, a strong decrease in emission intensity was observed in solution with smaller substituents (for Me and F). Viscosity- and temperature-dependent measurements of the F-DABate **5F[TBA]** showed an increasing emission intensity due to a more rigid environment. This can be attributed to the restriction of molecular motions, which is more favorable for the small substituents, and thus points to an aggregation effect. By inhibiting the rotational freedom and preventing the possibility of coplanar adjustment of the N_α substituent *via* the incorporation of the *o*-xylyl substituent, the fluorescence was also reduced. Quantum chemical calculations confirmed the important influence of the co-planarization of the N_α-aryl substituent in the excited state. Further calculations revealed an overall dominant intramolecular CT character, with the planarized N_α-Ph substituent as an electron donor for the DABate acceptor unit. Modification of the π backbone with a thieno unit led to an increased quantum yield in solution, which provides a promising strategy for future tailoring the properties of DABate fluorophores. Finally, we investigated the stability of this novel class of compounds, which revealed that both the N_β and aldimine positions play a significant role in determining overall stability. Guided by these principles, we were able to synthesize the first air- and moisture-stable C-DABate and are currently exploring the full potential of these and other further modified DABates.

Data availability

The data supporting this work is available in the ESI.†

Author contributions

L. W., J. C., H. H. and H. B. conceived the project. L. W. performed the synthesis and modification of all C-DABates except **7Ph[Li]**, with support of J. S. J. C. performed the synthesis of the F-DABate. T. K. performed the synthesis of the thiophene-fused compounds, including **7Ph[Li]**. J. C. performed the photophysical experiments. L. W. performed the quantum chemical calculations. J. C. and L. W. performed the decomposition studies. T. W., L. W., N. W., and M. M. performed the XRD experiments. L. W., J. C., H. H., and H. B. discussed the results. L. W. and J. C. wrote the manuscript. All authors have given approval to the final version of the manuscript.

Conflicts of interest

There are no conficts to declare.

Acknowledgements

We are grateful to Dr Ivo Krummenacher for insightful discussions and feedback on the manuscript. We also thank Dr Krzysztof Radacki for help with X-ray diffraction experiments, Dr Krzysztof Radacki and Lukas Endres for help with quantum-chemical calculations and Lukas Swoboda for HRMS measurements.

References

1 R. Karoui and C. Blecker, *Food Bioprocess Technol.*, 2011, **4**, 364–386.
2 A. Romani, C. Clementi, C. Miliani and G. Favaro, *Acc. Chem. Res.*, 2010, **43**, 837–846.
3 D.-E. Zacharioudaki, I. Fitilis and M. Kotti, *Molecules*, 2022, **27**, 4801.
4 M. Streit, M. Budiarta, M. Jungblut and G. Beliu, *Biophys. Rep.*, 2025, **5**, 100200.
5 N. Zhao, T. M. Williams, Z. Zhou, F. R. Fronczek, M. Sibrian-Vazquez, S. D. Jois and M. G. H. Vicente, *Bioconjugate Chem.*, 2017, **28**, 1566–1579.
6 T. Suzuki, T. Matsuzaki, H. Hagiwara, T. Aoki and K. Takata, *Acta Histochem. Cytochem.*, 2007, **40**, 131–137.
7 M. Shah, K. Thangaraj, M.-L. Soong, L. T. Wolford, J. H. Boyer, I. R. Politzer and T. G. Pavlopoulos, *Heteroatom Chem.*, 1990, **1**, 389–399.
8 E. Galbraith and T. D. James, *Chem. Soc. Rev.*, 2010, **39**, 3831–3842.

9 W. Zhang, G. Li, L. Xu, Y. Zhuo, W. Wan, N. Yan and G. He, *Chem. Sci.*, 2018, **9**, 4444–4450.
10 D. Wu, A. C. Sedgwick, T. Gunnlaugsson, E. U. Akkaya, J. Yoon and T. D. James, *Chem. Soc. Rev.*, 2017, **46**, 7105–7123.
11 N. Kwon, Y. Hu and J. Yoon, *ACS Omega*, 2018, **3**, 13731–13751.
12 D. M. Jameson, *Introduction to fluorescence*, CRC press, 2025.
13 E. Tervola, K.-N. Truong, J. S. Ward, A. Priimagi and K. Rissanen, *RSC Adv.*, 2020, **10**, 29385–29393.
14 N. K. Joshi, H. C. Joshi, R. Gahlaut, N. Tewari, R. Rautela and S. Pant, *J. Phys. Chem. A*, 2012, **116**, 7272–7278.
15 M. F. Anton and W. R. Moomaw, *J. Chem. Phys.*, 1977, **66**, 1808–1818.
16 D. Hu, R. Huang and Y. Fang, *Precis. Chem.*, 2025, **3**, 10–26.
17 D. Frath, J. Massue, G. Ulrich and R. Ziessel, *Angew. Chem., Int. Ed.*, 2014, **53**, 2290–2310.
18 J. Chorbacher, J. Klopf, A. Friedrich, M. Fest, J. S. Schneider, B. Engels and H. Helten, *Angew. Chem., Int. Ed.*, 2025, **64**, e202416088.
19 A. Treibs and F.-H. Kreuzer, *Adv. Cycloaddit.*, 1968, **718**, 208–223.
20 Y. Yang, X. Su, C. N. Carroll and I. Aprahamian, *Chem. Sci.*, 2012, **3**, 610–613.
21 F. L. Buguis, P. D. Boyle and J. B. Gilroy, *Dyes Pigm.*, 2022, **198**, 110002.
22 R. R. Maar and J. B. Gilroy, *J. Mater. Chem. C*, 2016, **4**, 6478–6482.
23 D. Cappello, F. L. Buguis, P. D. Boyle and J. B. Gilroy, *ChemPhotoChem*, 2022, **6**, e202200131.
24 D. Cappello, D. A. B. Therien, V. N. Staroverov, F. Lagugné-Labarthet and J. B. Gilroy, *Chem.–Eur. J.*, 2019, **25**, 5994–6006.
25 D. Cappello, A. E. R. Watson and J. B. Gilroy, *Macromol. Rapid Commun.*, 2021, **42**, 2000553.
26 M. C. Chang and E. Otten, *Chem. Commun.*, 2014, **50**, 7431–7433.
27 M.-C. Chang and E. Otten, *Inorg. Chem.*, 2015, **54**, 8656–8664.
28 M. C. Chang, A. Chantzis, D. Jacquemin and E. Otten, *Dalton Trans.*, 2016, **45**, 9477–9484.
29 G. Ulrich, R. Ziessel and A. Harriman, *Angew. Chem., Int. Ed.*, 2008, **47**, 1184–1201.
30 O. M. Kovtun, Y. V. Zatsikha and Y. P. Kovtun, *Chem. Heterocycl. Compd.*, 2023, **59**, 357–367.
31 J. W. Campbell, M. T. Tung, K. N. Robertson, A. A. Beharry and A. Thompson, *J. Org. Chem.*, 2023, **88**, 10655–10661.
32 M. Z. H. Kazmi, J. P. G. Rygus, H. T. Ang, M. Paladino, M. A. Johnson, M. J. Ferguson and D. G. Hall, *J. Am. Chem. Soc.*, 2021, **143**, 10143–10156.
33 S. Shimo, K. Takahashi and N. Iwasawa, *Chem.–Eur. J.*, 2019, **25**, 3790–3794.
34 E. A. Sarina, M. M. Olmstead, D. Kanichar and M. P. Groziak, *Acta Crystallogr., Sect. C:Struct. Chem.*, 2015, **71**, 1085–1088.
35 M. P. Groziak, A. D. Ganguly and P. D. Robinson, *J. Am. Chem. Soc.*, 1994, **116**, 7597–7605.
36 Y. Satta, R. Nishiyabu, T. D. James and Y. Kubo, *Tetrahedron*, 2017, **73**, 2053–2061.
37 S. Shimo, T. Nakamura, K. Takahashi, N. Toriumi and N. Iwasawa, *ChemPhotoChem*, 2022, **6**, e202100195.
38 L. Wüst, J. Chorbacher, T. Wellnitz, S. Nees, H. Helten and H. Braunschweig, *Chem. Sci.*, 2025, **16**, 7284–7293.
39 L. Wüst, L. Scheuring, T. Wellnitz, K. Radacki and H. Braunschweig, *Chem. Sci.*, 2025, **16**, 9934–9942.
40 M. Kim, C. H. Ryu, D. K. You, J. H. Hong and K. M. Lee, *ACS Omega*, 2022, **7**, 24027–24039.
41 U. P. Pandey and P. Thilagar, *Adv. Opt. Mater.*, 2020, **8**, 1902145.
42 J. Chorbacher, M. Maier, J. Klopf, M. Fest and H. Helten, *Macromol. Rapid Commun.*, 2023, **44**, 2300278.
43 S. Ji, J. Ge, D. Escudero, Z. Wang, J. Zhao and D. Jacquemin, *J. Org. Chem.*, 2015, **80**, 5958–5963.
44 K. Tanaka, H. Yamane, R. Yoshii and Y. Chujo, *Bioorg. Med. Chem.*, 2013, **21**, 2715–2719.
45 M. Maier, J. Chorbacher, A. Hellinger, J. Klopf, J. Günther and H. Helten, *Chem.–Eur. J.*, 2023, **29**, e202302767.
46 S. Gronowitz and A. Bugge, *Acta Chem. Scand.*, 1965, **19**, 1271–1285.
47 M. J. Frisch, G. W. Trucks, H. B. Schlegel, G. E. Scuseria, M. A. Robb, J. R. Cheeseman, G. Scalmani, V. Barone, G. A. Petersson, H. Nakatsuji, X. Li, M. Caricato, A. V. Marenich, J. Bloino, B. G. Janesko, R. Gomperts, B. Mennucci, H. P. Hratchian, J. V. Ortiz, A. F. Izmaylov, J. L. Sonnenberg, D. Williams-Young, F. Ding, F. Lipparini, F. Egidi, J. Goings, B. Peng, A. Petrone, T. Henderson, D. Ranasinghe, V. G. Zakrzewski, J. Gao, N. Rega, G. Zheng, W. Liang, M. Hada, M. Ehara, K. Toyota, R. Fukuda, J. Hasegawa, M. Ishida, T. Nakajima, Y. Honda, O. Kitao, H. Nakai, T. Vreven, K. Throssell, J. J. A. Montgomery, J. E. Peralta, F. Ogliaro, M. J. Bearpark, J. J. Heyd, E. N. Brothers, K. N. Kudin, V. N. Staroverov, T. A. Keith, R. Kobayashi, J. Normand, K. Raghavachari, A. P. Rendell, J. C. Burant, S. S. Iyengar, J. Tomasi, M. Cossi, J. M. Millam, M. Klene, C. Adamo, R. Cammi, J. W. Ochterski, R. L. Martin, K. Morokuma, O. Farkas, J. B. Foresman and D. J. Fox, Gaussian Inc., Wallingford CT, 2019.
48 J.-D. Chai and M. Head-Gordon, *Phys. Chem. Chem. Phys.*, 2008, **10**, 6615–6620.
49 F. Weigend and R. Ahlrichs, *Phys. Chem. Chem. Phys.*, 2005, **7**, 3297–3305.
50 A. D. Boese and N. C. Handy, *J. Chem. Phys.*, 2002, **116**, 9559–9569.
51 F. Weigend, *Phys. Chem. Chem. Phys.*, 2006, **8**, 1057–1065.
52 G. Haberhauer, R. Gleiter and C. Burkhart, *Chem.–Eur. J.*, 2016, **22**, 971–978.
53 T. Lu and F. Chen, *J. Comput. Chem.*, 2012, **33**, 580–592.
54 Z. Liu, T. Lu and Q. Chen, *Carbon*, 2020, **165**, 461–467.
55 R. Noyori and H. Takaya, *Acc. Chem. Res.*, 1990, **23**, 345–350.
56 J. P. M. António, J. I. Carvalho, A. S. André, J. N. R. Dias, S. I. Aguiar, H. Faustino, R. M. R. M. Lopes, L. F. Veiros, G. J. L. Bernardes, F. A. da Silva and P. M. P. Gois, *Angew. Chem., Int. Ed.*, 2021, **60**, 25914–25921.